17th World Conference on Earthquake Engineering, 17WCEE
Sendai, Japan - September 13th to 18th 2020

NUMERICAL ANALYSIS OF SEISMIC BEHAVIOR OF PLANE CONCRETE PIERS BASED ON THE DISTINCT ELEMENT METHOD

A. Furukawa [1], J. Kiyono [2], S. Yano [3] and K. Yoshikawa [4]

[1] *Associate Professor, Department of Urban Management, Kyoto University, furukawa.aiko.3w@kyoto-u.ac.jp*
[2] *Professor, Department of Urban Management, Kyoto University, kiyono.junji.5x@kyoto-u.ac.jp*
[3] *Master Student, Department of Urban Management, Kyoto University*
[4] *Master Student, Department of Urban Management, Kyoto University*

Abstract

It is reported that plain concrete piers of railroad bridges are damaged by earthquakes such as the 1978 Miyagi-ken-oki earthquake and the 2004 Niigata-ken Chuetsu earthquake. The typical damage pattern of plain concrete piers during earthquakes is horizontal gap at the cold joint of a pier and falling of concrete pieces from the pier under the cold joint. It is necessary to develop a numerical analysis method suitable for plain concrete piers to evaluate their seismic safety against the future earthquakes. With this background, this study proposes the refined distinct element method (refined DEM) for the dynamic analysis of plain concrete piers.

First, we found that the original refined DEM has a problem of overestimating friction properties. Therefore, the method was proposed to accurately simulate the friction coefficient by modifying the arrangement of springs.

Next, we found that the modified refined DEM has a problem in the accuracy of rotational angle. Therefore, we proposed the method to improve the accuracy of rotational angle by modifying the arrangement of springs again. Finally, we could develop the refined DEM which can simulate the both friction behavior and rotation behavior accurately.

Next, a shaking table test of a plain concrete pier was simulated, and the analytical and experimental results were compared. In the analysis, two acceleration histories with different peak acceleration values were input. In the case of smaller accelerations where the specimen suffered slight failure, it was found that the horizontal dislocation and failure occurrence situation was simulated with good accuracy. On the contrary, in the case of larger accelerations where the specimen suffered severe damage, it was found that the damage occurrence situation was barely simulated.

Therefore, we modified the nonlinearity models of springs. We proposed a simple constitutive model suitable for DEM to express tensile softening and compressive softening suitable for concrete structures. Using this constitutive model, the dynamic behavior of a plain concrete pier during the shaking table was simulated. By improving the constitutive model in addition to the spring arrangement model, we could improve the accuracy of failure behavior.

Keywords: numerical analysis; plain concrete pier; seismic behavior; refined DEM

1. Introduction

In Japan, plain concrete piers were constructed prior to 1914 when the design standard for reinfored concrete structures for railway was prescried, and they are still in use in the railroad bridges of conventional lines. Plain concrete piers have been damaged by earthquakes such as the 1978 Miyagi-ken-oki earthquake and the 2004 Niigata-ken Chuetsu earthquake [1, 2, 3, 4]. The typical damage is horizontal gap at the cold joint of a pier and falling down of concrete pieces from the pier under the cold joint. Fig. 1 shows a pier 14 of Uonogawa bridge damaged by the 2004 Niigata-ken Chuetsu earthquake [3]. From the figure, it can be seen that horizontal gap is about 30-40 cm and concrete pieces are fallen down from the edge of the pier under the cold joint.

It is necessary to understand the damage occurrence mechanism and develop effective seismic measures to prevent serious damage in the future earthquake. In this study, the refined DEM was first improved by changing the arrangement of springs so that the sliding and rotation behavior match the theoretical values. Then a shaking table test of a plain concrete pier conducted by West Japan Railway Company in January 2015 was simulated by using the refined DEM. The validity of the numerical simulation was evaluated by comparing the numerical and experimental results of the seismic behavior.

Fig. 1 – Uonogawa Bridge damaged during the 2014 Niigata-ken Chuetsu Earthquake [3]

2. Analysis Method

2.1 Refined DEM

This study employs a refined DEM [5] to simulate a series of structural dynamic behaviors from elastic to failure to collapse phenomena. A structure is modeled as an assembly of rigid elements, and interaction between elements is modeled with multiple springs and multiple dashpots that are attached to the surfaces of elements.

Fig. 2 (a) shows a spring for computing the restoring force (restoring spring), which models the elasticity of elements. The restoring spring is set between continuous elements. Fig. 2 (b) shows a spring and dashpot for computing the contact force (contact spring and dashpot) and modeling the contact, separation and recontact between elements. The dashpots are introduced to express energy dissipation due to the contact. Structural failure is modeled as breakage of the restoring spring at which time the restoring spring is replaced with a contact spring and a contact dashpot. Structural collapse behavior is obtained using these springs and dashpots.

The surface of an element is divided into small segments. In the original Refined DEM, the surface of element was devided as shown in Fig. 3(a). But in this study, we introduce new sprig arragenemnts as shown in Fig.3(b) and Fig.3(c) to increase the accuracy of sliding behavior and rotation behavior. The black points indicate the representative point of each segment, and the relative displacement or contact displacement between elements is computed for these points. Such points are referred to as contact points or master points in this study. One restoring spring and one combination of contact spring and dashpot are attached to one

segment at each of the representative points. The spring constant for each segment is derived on the basis of the three-dimensional stress–strain relationship of the material and the segment area. Forces acting on each element are obtained by summing the restoring force, contact force and other external forces such as the gravitational force and inertial force of an earthquake. The behavior of an element consists of the translational behavior of the center of gravity and the rotation behavior around the center of gravity. The translational and rotation behaviors of each element are computed explicitly by solving Newton's law of motion and Euler's equation of motion.

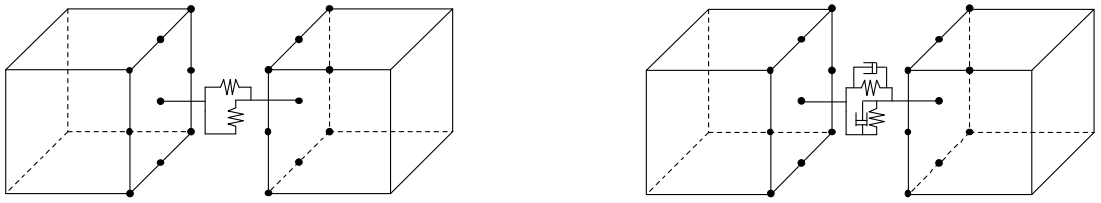

(a) Restoring spring (b) Contact spring and dashpot

Fig. 2 – Spring and dashpot between elements

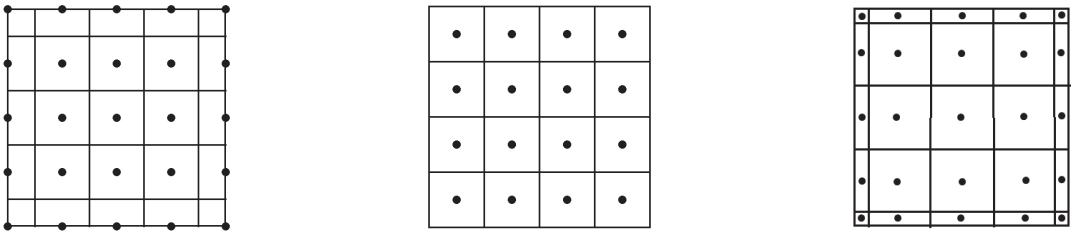

(a)Original arrangement A (b) Arrangement B (c) Arrangement C

Fig. 3 – Segments and contact points

2.2 Spring constant of each element

There are two types of springs, namely restoring and contact springs. It is considered that each segment has its own spring. The springs are set for both the normal and shear directions of the surface. The spring constants per area in the normal and shear directions, k_n and k_s, are obtained as follows.

$$k_n = \frac{E}{(1-\nu^2)\ell}, \quad k_s = \frac{E}{2(1+\nu)\ell} \tag{1}$$

where E is Young's modulus, ν is Poisson's ratio, and ℓ is the distance from the surface at which the spring is connected to the center of gravity.

2.3 Modeling of elastic behavior

It is assumed that two elements, A and B, are continuous, and that a contact point of element A is continuous with element B. Let G_A and G_B be the centers of gravity of elements A and B respectively. Let ℓ_A be the distance from G_A to the surface of element A in contact. Let ℓ_B be the distance from G_B to the surface of element B in contact. Let E_A and E_B be Young's moduli and ν_A and ν_B be Poisson's ratios of elements A and B.

The spring constants per area for the elements A and B are obtained from Eq. (1). Assuming that these springs are connected in series, the spring constants between elements per area, $\bar{k}_n$ and $\bar{k}_s$, are

$$\bar{k}_n = \frac{1}{\frac{\ell_A}{E_A/(1-\nu_A^2)} + \frac{\ell_B}{E_B/(1-\nu_B^2)}}, \quad \bar{k}_s = \frac{1}{\frac{\ell_A}{E_A/2(1+\nu_A)} + \frac{\ell_B}{E_B/2(1+\nu_B)}}. \tag{2}$$

The spring constant between elements connected by mortar is also obtained in a similar manner. For example, in masonry structures, bricks are often connected with mortar. In such cases, the spring constant per area between elements (bricks) is obtained as

$$\bar{k}_n = \frac{1}{\frac{\ell_A - t_M/2}{E_A/(1-\nu_A^2)} + \frac{t_M}{E_M/(1-\nu_M^2)} + \frac{\ell_B - t_M/2}{E_B/(1-\nu_B^2)}}, \quad \bar{k}_s = \frac{1}{\frac{\ell_A - t_M/2}{E_A/2(1+\nu_A)} + \frac{t_M}{E_M/2(1+\nu_M)} + \frac{\ell_B - t_M/2}{E_B/2(1+\nu_B)}} \tag{3}$$

where t_M is the mortar thickness and E_M is Young's modulus and ν_M is Poisson's ratio of the mortar. The normal direction of forces is the direction perpendicular to the surface of the master point of element A.

Let σ and τ be the normal and shear stresses acting at the contact point, and u_n and u_s be the relative displacements between the adjacent master and slave points in the normal and shear directions. The relation between traction (σ, τ) and relative displacements (u_n, u_s) is then written as

$$\sigma = \bar{k}_n u_n, \quad \tau = \bar{k}_s u_s. \tag{4}$$

The method cannot handle the poisson's effect since it considers the contact between two elements.

2.4 Modeling of failure phenomena

The elastic behavior of structures is demonstrated by the multiple restoring springs between continuous elements until the restoring force of a spring reaches its elastic limit. The elastic limits are modeled using criteria of tension, shear and compression failure. When a spring reaches one of these limits, it is judged that failure has occurred at the segment of the spring. After the failure, the restoring spring is replaced with a contact spring and dashpot at this segment. The method can trace the expansion of failure between elements. The three failure modes—namely, tension, shear and compression failure modes—are defined as follows.

2.4.1 Tension failure mode

In the tension failure mode, the parameter considered is the tensile strength f_t. When the normal stress of a spring σ exceeds the tensile strength, the restoring spring is assumed to be broken by the tension failure. The yield function has the following form (Fig. 4).

$$f_1(\sigma) = \sigma - f_t \tag{5}$$

The normal restoring stress cannot exceed this limit.

2.4.2 Shear failure mode

For the shear failure mode, the Coulomb friction envelope is used. The parameters considered are the bond strength c and friction angle ϕ. The yield function has the following form (Fig. 4).

$$f_2(\sigma) = |\tau| + \sigma \tan\phi - c \tag{6}$$

The shear restoring stress cannot exceed this limit.

2.4.3 Compression failure mode

For the compression mode, an ellipsoid cap model is used. The yield function has the form (Fig. 4) as

$$f_3(\sigma) = \sigma^2 + C_s\tau^2 - f_m{}^2 \tag{7}$$

where f_m is the compressive strength and Cs is the material model parameter. Cs = 9 is adopted on the basis of past research [6]. When the restoring stress exceeds this limit, both the normal and shear restoring stresses are reduced in the same proportion to meet this limit.

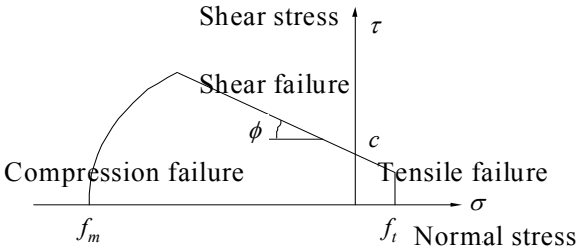

Fig. 4 – Failure judgment

2.5 Modeling of contact and recontact between elements

If a segment of an element is in contact with another element with which the segment is not continuous via the restoring spring, the contact spring and dashpot generate the contact force. Contact between a segment and the surface of another element is detected at each time step for all segments that are not continuous with other elements via a restoring spring. The spring constant and the contact forces in the normal and shear directions are calculated in the same manner as for the restoring force. The differences from the case for the restoring force are that the contact force is generated only while the compression force acts and that the shear force is bounded by the friction limit.

$$\tau = \sigma \tan\phi \tag{8}$$

where ϕ is the friction angle. The dashpot is introduced to express the energy dissipation of the contact. The damping coefficient per area is calculated as follows.

$$c_n = 2h_n\sqrt{m_{ave}k_n}\ ,\quad c_s = 2h_s\sqrt{m_{ave}k_s} \tag{9}$$

where h_n and h_s are the damping constants for the normal and shear directions. m_{ave} is the equivalent mass per area relevant to this contact. In this study, m_{ave} is calculated as

$$m_{ave} = \rho_A \ell_A + \rho_B \ell_B \tag{10}$$

where ρ_A and ρ_B are the mass densities of elements A and B. The damping constants should be evaluated according to the properties of the elements, but this study adopts critical damping (h_n = h_s = 1.0) by considering that most structural components tend not to bounce greatly and their oscillation tends to disappear quickly when they collide with each other.

2.6 Equations of Motion

The equations of motion can be constructed using the restoring and contact forces and other external forces. The motion of each element is obtained by solving the two equations of motion. One is the equation for the translational motion of the center of gravity, and the other is the equation for the rotational motion around the center of gravity. By solving the equations of motion step by step, the position of each element can be traced, and the whole structural behavior can be obtained.

3. Arrangement of Springs

3.1 Sliding Behavior

When the shaking table test is simulated by using the Refined DEM with the conventional spring arrangement A as shown in Fig.3(a), it is found that the friction coefficient is overestimated and the damage to the lower concrete than the cold joints is overestimated compared to the actual shaking table test results.

It is found that the interlocking between elements causes this problem. In Fig.5, upper and lower two elements represent upper and lower elements at the joint, respectively. In the Refined DEM, each element is a rigid body and does not deform. The deformation is modeled as an overlapping between elements.

When a gravity force acts on the model, the upper elements overlaps with the lower elements and a reacting force is generated. Moreover, when a horizontal force in the right direction acts on the upper elements, a reacting force is generated as shown in Fig. 5.

On the other hand, if the uppdr and lower elements are divided into two elements, a compressive force is generated between upper left and lower right element. This causes the increase of the coefficient of friction, as shown in Fig. 6(a). Moreover, the generated force acts on right bottom elements. This causes the damage of the elements, as shown in Fig. 6(b).

Fig. 3(b) shows a model proposed in this research. Springs are not set at the vertex nor edges but set only to the surfaces of the element in the arrengement B. This model can solve the previous problem.

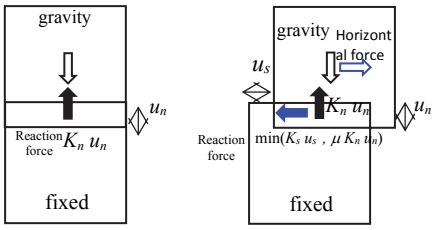

Fig. 5 – Forces acting between two elements

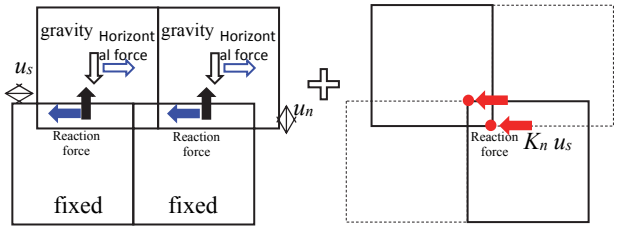

(a) The reason why friction coefficient is overestimated in the numerical analysis

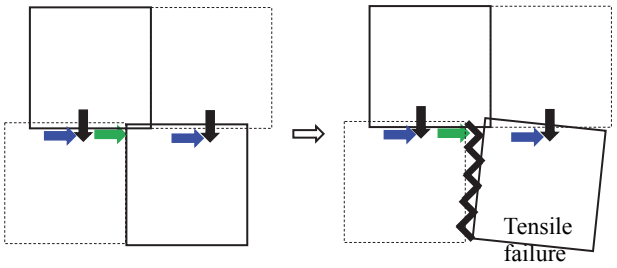

(b) The reason why the lower elements are easy to be damaged in analysis

Fig. 6 – The reason why the numerical analytical result is different from that of the experiment

3.2 Rotation Behavior

The conventional refined DEM didn't reproduce the friction coefficient theoretically because the vertexes of the elements got caught when the concrete above the cold joint slid. By introducint the new spring arrangement as shown in Fig.3(b), this problem was eliminated, and the friction coefficient was reproduced theoretically.

However, it was found that the spring arrangement B has the problem that the resisting moment was underestimated, and rotation motion was not reproduced well as shwon in Fig.7(a). Therefore, in this study, the springs at the end were set at a position closer to the vertex and new spring arragnement C as shown in Fig.3(c) is proposed to eliminate the undestimation of resising moment as shown in Fig.7(b). If the length of edges of elements is 1, the springs were set at the location 0.001 from the end. Then, we also set springs at the center of the segmented surface. By this improvement, it was confirmed that the theoretical solution and numerical solution agreed in both sliding and rocking behaviors. The reliability of the refined DEM was confirmed.

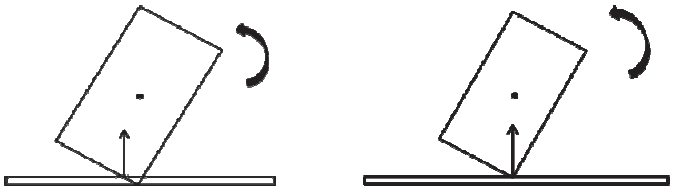

(a) Spring arrangement B (b) spring arrangement C

Fig. 7 – Resisting moment

4. Numerical Analysis of Shaking Table Test

4.1 Specimen and Numerical Model

Fig.8 shows the specimen of shaking table test [7] and the numerical analysis model. The width, depth and height of footing are 2.29m, 1.5m and 0.6m, respectively. The width, depth and height of the pier are 1.45m, 0.66m and 1.65m, respectively. The height of the cold joint of a pier is 0.4m. The element size varies from part to part. The area with the width of 20 cm at both ends was assumed to be damageable and divided with smaller elements. However, the other parts were assumed to be undamageable and divided with larger elements. We simulated the test with two models as shown in Fig.9. In model 1, the element width of the damaged part was basically 5 cm. In model 2, the element width of the damaged parts was basically 2.5 cm. The height of the elements was 5 cm for the lower concrete and the first layer of the upper concrete, and 10 cm for the uppper concrete except the first layer. We didn't divide the pier in the depth direction. The width, depth, and height of the steel weight are 0.6m, 0.45m and 0.525m, respectively.

The material properties were determined based on the element test result of the specimen [7]. The density, Young's modulus, Poisson's ratio and the compressive strength of the concrete are 2.3×10^{3}kg/m^2, 2.2×10^{10}N/m^2, 0.2 and 2.784×10^{7}N/m^2, respectively. The tensile and shear strength are assumed to be one tenth and one quarter of the compressive strength, respectively. The mass, Young's modulus and Poisson's ratio of the steel weight are 810 kg, 2.0×10^{11}N/m^2 and 0.3. The damping coefficient is 1.0 as critical damping. The tensile strength of the joint is 0 because the joint's surface was processed and flat. Also, the friction coefficient is 0.64 based on the element test result.

4.2 Input Acceleration

In shaking table test, the waveform which was transformed according to the similarity law from L2 earthquake motion (spectrum II) of railway structure design standard was used [7]. The amplitude was also scaled to change the level of excitation. In this simulation, we used two cases of maximum acceleration 1000 and 1200gal, in which failure of concrete edge under the cold joint occurred and input three seconds from 11.895 seconds to 14.895 seconds with large amplitude of the acceleration waveform measured on the vibration test as shown in Fig.10.

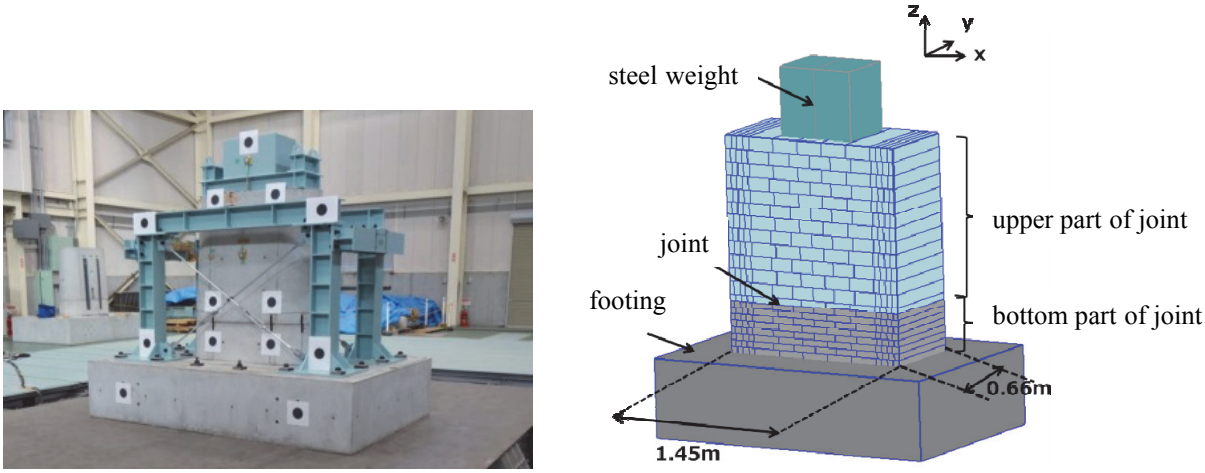

Fig. 8 – Specimen and the numerical analysis model [7]

(a) Model 1 (b) Model 2

Fig. 9 – Two models with different element size

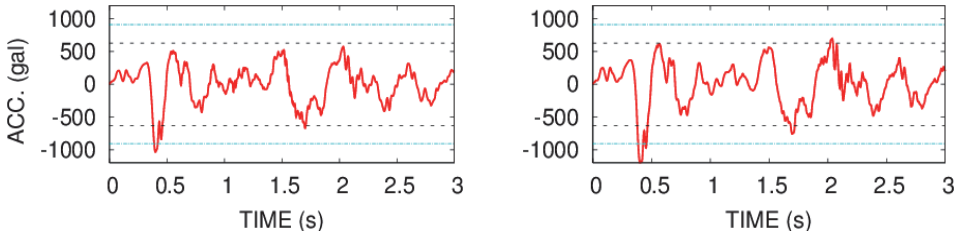

(a) 1000 gal case (b) 1200 gal case

Fig. 10 – Input accelerations (Blue dot line indicates the acceleration at which the sliding starts and blue line indicates the acceleration at which the rocking starts) [7]

3.5 Results

3.5.1 Model 1

Fig.11 shows the dyanmic behavior of model 1 during 1000gal and 1200 gal input. In the case of 1000gal input of model 1, the concrete above the cold joint slided to right direction, but the edge under the cold joint didn't break, and the rocking didn't occur. In case of 1200gal input of model 1, the right edge under the cold joint got broken, and the rocking occurred slightly. The damage didn't occur in the case of 1000gal input because the sliding displacement was about 2 cm and that is smaller than the element width. On the other hand, in the case of 1200gal input, sliding dispalcemetn was about 4 cm which is larger than the element

width, therefore the damage under the cold joint occurred. However, the damage did not ocure in the the left edge under the cold joint. The reason was that after sliding to the right direction, the concrete above the cold joint didn't slide to the left direction. Fig.12 shows the comparison of the horizontal gap of the cold joint and the rotation angle around the cold joint between the numerical analysis and the experiment.

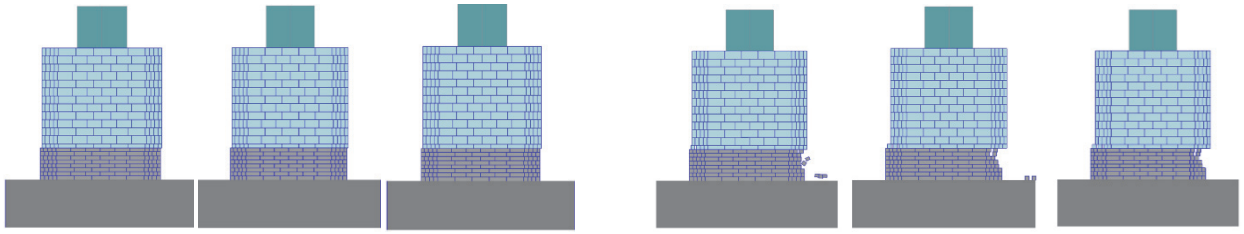

(a)1000 gal(0.65 s, 1.9 s, and 2.5 s from the left) (b)1200 gal(0.70 s, 1.9 s, and 2.5 s from the left)

Fig. 11 – Result of Model 1

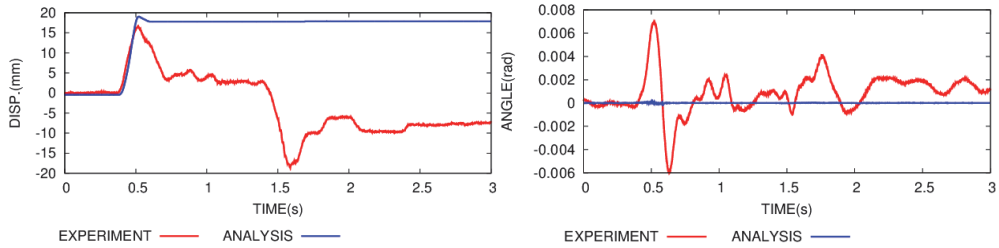

(a) 1000gal

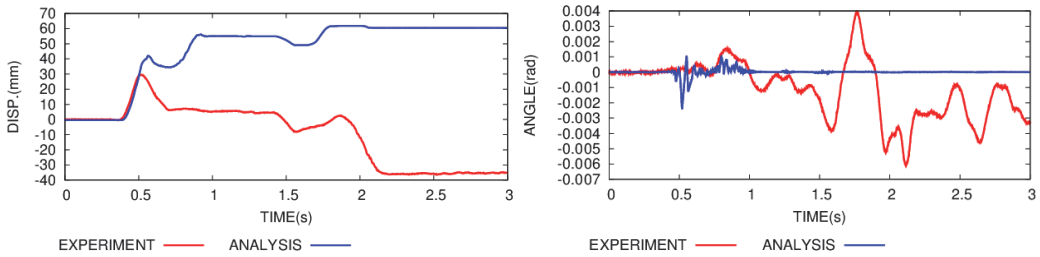

(b) 1200gal

Fig. 12 – Horizontal gap (left) and rotation angle (right) for model 1

3.5.2 Model 2

Fig.13 shows the dyanmic behavior of model 1 during 1000gal and 1200 gal input. Since the element width is smaller, the damage to the both edges under the cold joint occurred for both 1000 gal and 1200 gal input. In the case of 1000gal input, the damage occurence mechanism of the concrete edge under the cold joint was reproduced, and the rocking occurred better than the case of model 1. However, in the case of 1200gal, the concrete above the cold joint also get damaged. The reason is probably that the width of the elements was different between the damageable and undamageable parts.

As shown in Fig.14, the time history of the horizontal gap was in good agreement between experimental and analysis results in the beginning, but they didn't match once the failure started. The rotation angle was underestimated.

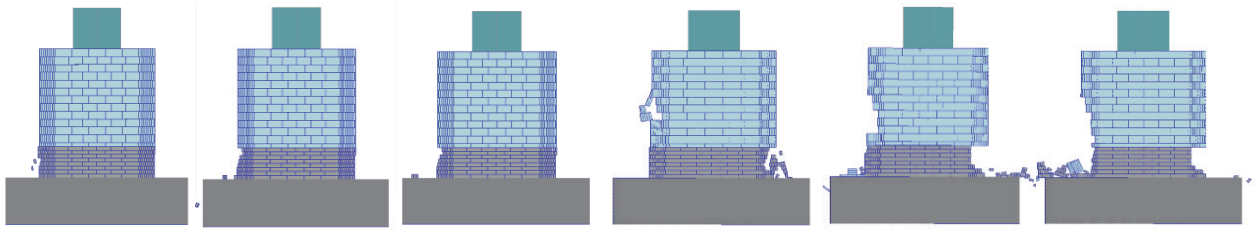

(a)1000 gal(0.7 s, 1.9 s, and 2.5 s from the left) (b)1200 gal(0.70 s, 1.9 s, and 2.5 s from the left)

Fig. 13 – Result of Model 2

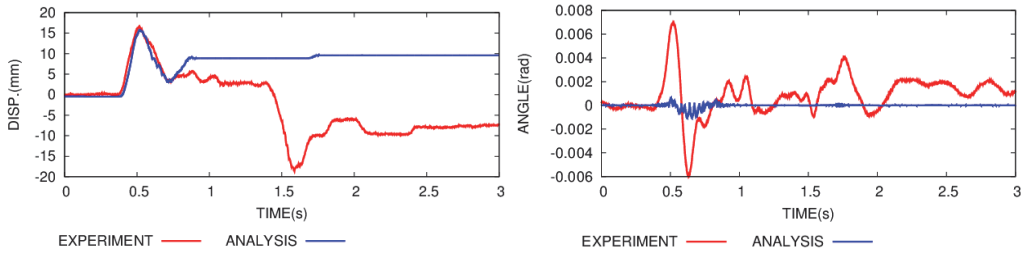

(a) 1000gal

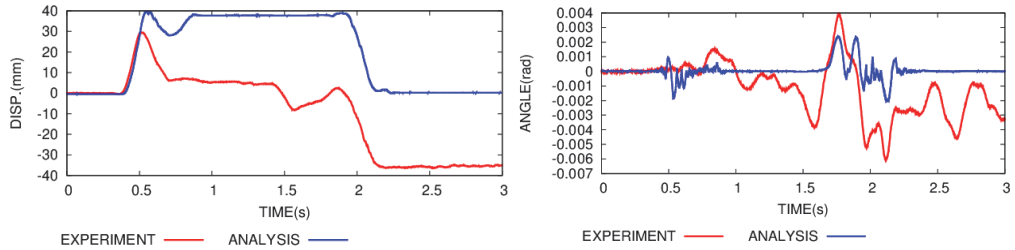

(b) 1200gal

Fig. 14 – Horizontal gap (left) and rotation angle (right) for model 2

3.6 Modification of stress-starin relationship

3.6.1 Skelton curve

Fig.15(a) indicates the stress-strain relationship of the original refined DEM. In this study, the stress-strain relationship shown in Fig. 15(b) was introduced. In the tension side, tension softening was considered and $\varepsilon_{tmax} = \varepsilon_t$ was used. In the compressive side, compression softening was introduced and $f_{c2} = 1/2\, f_c$ was used. Moreover, hysteresis curve was introduced.

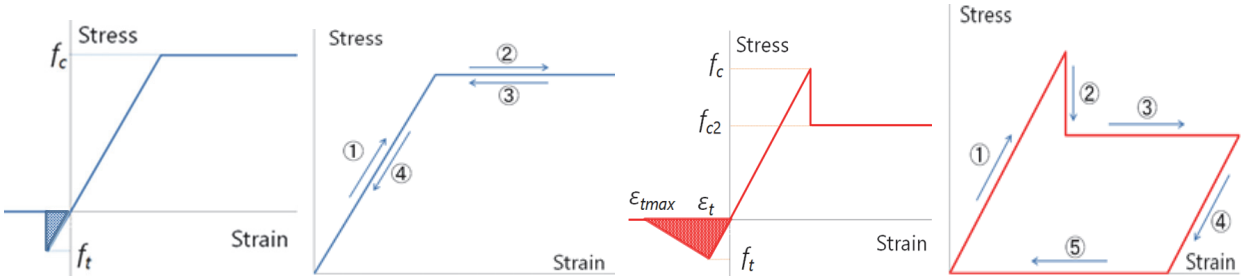

(a)Previous model (b) Modified model

Fig. 15 – Stress-strain relationship (left: Skelton curve, right: Loaing and unloading pass (compression side))

3.6.2 Model 2 with new stress-stain relationship

The result of model 2 with the new stress-strain relationship is shown in Fig.16 and Fig.17. The damage occured only to the concrete edge lower than the cold joint. No damage occured to the concrete edge above the cold joint. This is the same damace occurence with the actual experiment. The reproducibility of the horizontal gap was not improved, but the reproducibility of the rotation angle was slightly improved. In this way, by introducing the new stress-strain relationship considering the tensile softening, compression softening and the hysteretic curve in the compresion side, the accuracy of the numerical simulation could be improved.

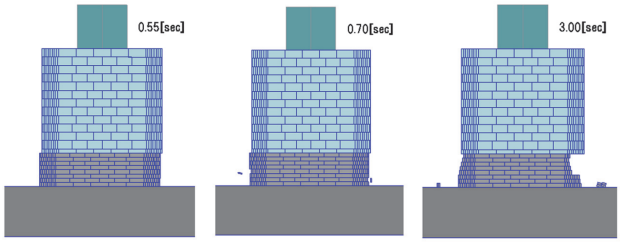

(a)1200 gal(0.550 s, 0.7 s, and 3 s from the left)

Fig. 16 – Result of Model 2 with new stress-stain relationship

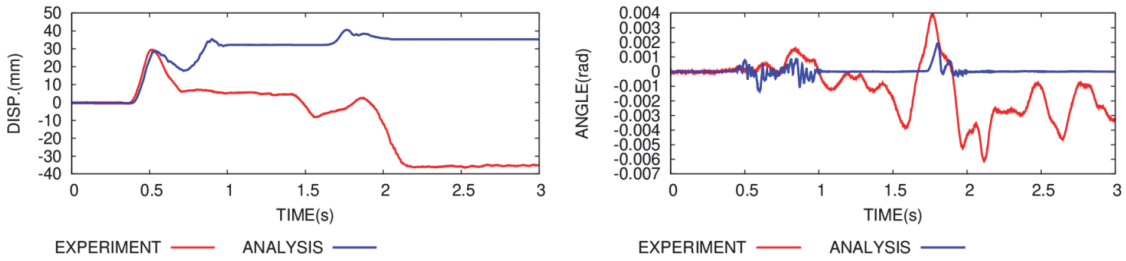

(a) 1200gal

Fig. 17 – Horizontal gap (left) and rotation angle (right) of model 2 with new stress-stain relationship

3.7 Damage occurence mechanism of concrete under the cold joint

Fig.18 shows the damage occurrence mechanism of concrete at the edge under the cold joint. First, the concrete above the joint starts sliding to right direction (positive *x* direction). Then, the specimen above the cold joint rotates clockwise and damage occures at the right edge under the cold joint. Next, the specimen above the cold joint slides to left direction and rotates unticlockwise. Then, the left edge under the cold joint is broken. Finally, the both edges under the cold joint are got broken.

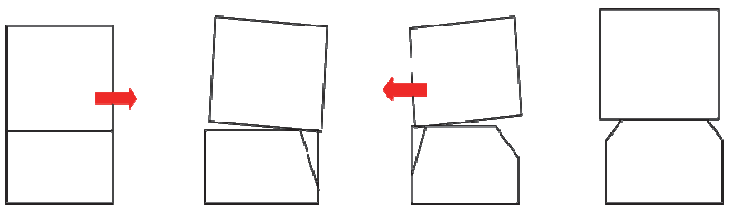

Fig. 18 – Damage occurence mechanism of concrete edge under the cold joint

4. Conclusions

In this study, we improved the spring arranement model of the refined DEM so that the both friction behavior and rotaion behavior can be simulated accurately.

By using this new spring arrangement model, we simulated the dynamic behavior of a miniture plain concrete pier during the shaking table test. The findings are shown below.

(1) In the case of 1000 gal input, the damage to the concrete edge under the cold joint occured in the shaking table test. However, the numerical analysis using model 1 could not reroduce the damage occurence. The reason was found that the element width of model 1 is larger than the horizontal dislocation and the element width was not small enough to reproduce the damage occurence.

(2) The numerical analysis using model 2 with smaller element width could reproduce the damage to the concret edge under the cold joint as observed during the shaking table test. The initial horizontal gap showed good agreement between the shaking table test and the numerical analysis, but the agreement of the rotation angle was not good.

(3) In the case of 1200gal input to mode 2, the concrete above the cold joint also got broken whih was not observed during the shaking table test.

(4) Therefore, we modified the constitutive model of springs. We proposed a simple stress-strain relationship suitable for DEM to express tensile softening and compressive softening suitable for concrete structures. Using this constitutive model, the dynamic behavior of a plain concrete pier during the shaking table was simulated. By improving the constitutive model in addition to the spring arrangement model, we could improve the accuracy of failure behavior even in the case of 1200gal input to model 2.

5. Acknowledgements

We were allowed to use the results of shaking table test by West Japan Railway Company.

6. References

[1] Hakuno, M, Fujino Y, Katada T, Matsubara K (1979): Report of damage survey of 1978 Off Miyagi Prefecture earthquake, *Bulletin of the Earthquake Research Institute*, University of Tokyo, **54**, 351-398.

[2] Morikawa H, Fukushima Y (2004): Damage to civil engineering structures during 2004 Niigata-ken Chuetsu earthquake, *Research Reports on Earthquake Engineering*, Center for Urban Earthquake Engineering (CUEE), Tokyo Institute of Technology, **92**, 43-56.

[3] Disaster Investigation Team of Kyushu Institute of Technology (2000): Preliminary report of second damage survey of 2004 Niigata-ken Chuetsu earthquake, http://www.civil.kyutech.ac.jp/pub/kosa/ijikenHP/tyuuetujisin20041025.pdf [Last accessed: Sept 4, 2019].

[4] Second survey team of Kanto branch of JSCE (2004): Damage survey of Niigata-ken Chuetsu earthquake, Survey report of second survey team of Kanto Branch of JSCE, http://www.fps.chuo-u.ac.jp/~hrsk/earth/2004-niigata/files /nogami.pdf [Last accessed: Sept 4, 2019].

[5] Furukawa A, Kiyono J, Toki K (2011): Proposal of a Numerical Simulation Method for Elastic, Failure and Collapse Behaviors of Structures and its Application to Seismic Response Analysis of Masonry Walls, *Journal of Disaster Research*, **6**(1).

[6] Lourenco P.B (1994): Analysis of masonry structures with interface elements, theory and applications, *TU-DELFT report*, Delft University of Technology, Faculty of Civil Eng., 03-21-22-0-01.

[7] Railway Technical Research Institute (2015): Confirmation Report, Confirmation test on earthquake proof countermeasure against plain concrete piers.

